PAPER • OPEN ACCESS

Electron transport barrier and high confinement in configurations with internal islands close to the plasma edge of W7-X

To cite this article: N. Chaudhary *et al* 2024 *Nucl. Fusion* **64** 106038

OPEN ACCESS
IOP Publishing | International Atomic Energy Agency
Nuclear Fusion
Nucl. Fusion **64** (2024) 106038 (9pp)
https://doi.org/10.1088/1741-4326/ad703e

Electron transport barrier and high confinement in configurations with internal islands close to the plasma edge of W7-X

N. Chaudhary[1,*], M. Hirsch[1], T. Andreeva[1], J. Geiger[1], R.C. Wolf[1], G.A. Wurden[2] and the W7-X Team[a]

[1] Max-Planck-Institut für Plasmaphysik, Greifswald, Germany
[2] Los Alamos National Laboratory, Los Alamos, NM, United States of America

E-mail: neha.chaudhary@ipp.mpg.de

Received 15 January 2024, revised 6 August 2024
Accepted for publication 16 August 2024
Published 3 September 2024

Abstract

The low magnetic shear in the Wendelstein 7-X (W7-X) stellarator makes it feasible to shape the separatrix by the large islands constituting an island-divertor, and this can be exploited to access various magnetic configurations, including samples of different internal island sizes and locations. To investigate the configuration effects on the plasma confinement, a configuration scan was performed by changing the coil currents to vary the rotational transform between values $5/4$ and $5/6$ at the plasma boundary with different power levels (2, 4, 6 MW) of electron cyclotron resonance heating (ECRH) at a maximum plasma density of $8 \times 10^{19}\,\mathrm{m}^{-2}$. neutral beam injection (NBI) heating was also applied during some configurations of the scan to create a density ramp and access high densities beyond the X2 ECRH cutoff. For the magnetic configurations, where the $5/5$ and $5/6$ island chains were moved closer to separatrix but remaining inside the last closed flux surface, the electron cyclotron emission shows that an electron temperature, T_e, pedestal develops already during ECRH heated plasma buildup phase indicating a transport barrier, and the barrier sustains irrespective of changed plasma heating conditions such as NBI in the later part of discharge. The transport barrier is broken by subsequent fast crashes, observed with multiple plasma diagnostics with characteristics such as tokamak edge localized modes, and the corresponding crash amplitude and frequency vary with plasma pressure. The impact of the transport barrier on plasma confinement can be seen through the increased core T_e profile, which could be responsible for the overall increase in the stored diamagnetic energy by approximately 10% for these configurations. After the plasma heating is terminated, a backwards transition to a degraded confinement state is also observed. These observations indicate a configuration triggered high confinement mode in low shear W7-X. This work focuses on the occurrence of this transport barrier for different magnetic configurations and its relation to internal magnetic islands.

[a] See Grulke *et al* 2024 (https://doi.org/10.1088/1741-4326/ad2f4d) for the W7-X Team.
[*] Author to whom any correspondence should be addressed.

Keywords: transport barrier, internal magnetic islands, island localized modes, high confinement, stellarator, pedestal

(Some figures may appear in colour only in the online journal)

1. Introduction

Plasma edge conditions determine confinement both in the tokamak and stellarator [1–3], and for low-magnetic shear stellarators, the details of the magnetic configuration such as the edge rotational transform have been found to be a leading quantity [4–6]. Wendelstein 7-X (W7-X) is an optimized stellarator for low magnetic shear topology with an operational goal of 30 min of steady state detached plasma heated with 10 MW of electron cyclotron resonance heating (ECRH) and interlaced with 10 s high-power phases of neutral beam injection (NBI) [7–9]. The flexibility of the device allows us to exploit various magnetic configurations, island sizes and locations, including samples where these major rational islands are shifted inward such that they are fully embedded in closed flux surfaces even toward the plasma edge. The internal islands exist in vacuum as a resonant perturbation of the otherwise five-fold symmetry of the fully external magnetic field in W7-X. An experimental proof is that they can be visualized with an electron beam in vacuum [10] and the islands have fixed positions. They can be shifted radially further outwards or inward from their normal position by changing the rotational transform of the vacuum magnetic field [11]. In the normal position of the standard configurations, these islands are used for the island-divertor operation, which is one possible divertor concept, in particular for low-shear devices [12–14]. However, there are additional coils, the control coils, which allow a change to the island width or the ability to move them poloidally to some degree, thus allowing for a sweeping of the divertor footprints to mitigate the local heat-loads on the divertor targets. The configuration effects on the plasma confinement were realized and a configuration scan was performed by changing the coil currents to vary the rotational transform between $5/4$ and $5/6$ at the plasma boundary with ECRH and NBI [11, 15]. The corresponding configurations alongside the experimental setup are described in the following section.

2. Experimental setup

The iota scan experiments were performed by varying the radial location of the internal-island chain, making it possible to access various island-divertor and limiter configurations with both ECRH and NBI heating, and a detailed description of the configuration scan can be found in [11, 15]. The plasma startup and heating was done with ECRH in the steps of 2, 4, 6 MW with maximum plasma density of $8 \times 10^{19}\,\mathrm{m}^{-2}$, such as to have controlled plasma heating and density during the scan. The iota scan was carried out shot by shot via changing control coil currents, while keeping the on-axis magnetic field fixed. Additionally, some configurations from the iota scan were also tested with NBI heating to access a wider plasma parameter regime beyond X2 ECRH cutoff densities.

Table 1 shows the experimental details such as the iota at the center, ι_0, and at the plasma edge, ι_e, at $\beta = 0$ of some sample configurations which were accessed during the iota scan and will be discussed in this paper. Figure 1 shows the vacuum Poincaré plots of three selected configurations from the iota scan alongside a bean-shaped plasma cross-section in W7-X. The overall toroidal currents for these experiments at the chosen timestamps in the shot (approximately at 2–3 s) are rather small [16], and, hence, do not change the equilibrium significantly. The iota scan experiments varied the coil currents; hence, the rotational transform between nominal edge values 5/4, 5/5 and 5/6, such that the plasma edge is determined by major island chains resembling 4, 5 or 6 islands, respectively. Figure 1 shows three sample configurations from the scan: (left) the standard configuration with the internal name, EJM, with $\iota_0 = 0.858$ which is used for routine operations and has the 5/5 island chain forming the separatrix making it a proper island-divertor configuration; (middle) the high-confinement configuration, internal name FMM, with $\iota_0 = 0.911$ where the 5/5 island chain is now *inside* the LCFS; (right) the high-iota configuration with internal name FTM, and $\iota_0 = 1.012$ which has the 5/4 islands at the boundary forming also a proper island divertor configuration. A systematic comparison of the stored diamagnetic energy, W_{dia}, for these configurations with the highest values for the FMM (high-confinement configuration) is provided in [11].

The electron cyclotron emission (ECE) diagnostic is used to track the electron temperature, T_e, gradients. A 32 channel heterodyne radiometer measures the second harmonic extraordinary mode from 120 to 160 GHz covering the plasma width with a temporal resolution on the order of few μs, which is sufficient to resolve the fast magnetohydrodynamic events, temperature crashes, and related gradient changes [17]. The line of sight of the ECE diagnostic is close to the bean-shaped section as shown in the Poincaré plots of figure 1, such that along the line of sight the 5/5 island chain in the high-confinement configuration is cut at an O-point at the low field side and an X-point at the high field side. Equilibrium calculations for the high-confinement configuration with plasma β of 1% and 2% show that the location of the island-chain (with the island width approximately 8 cm) does not change significantly with

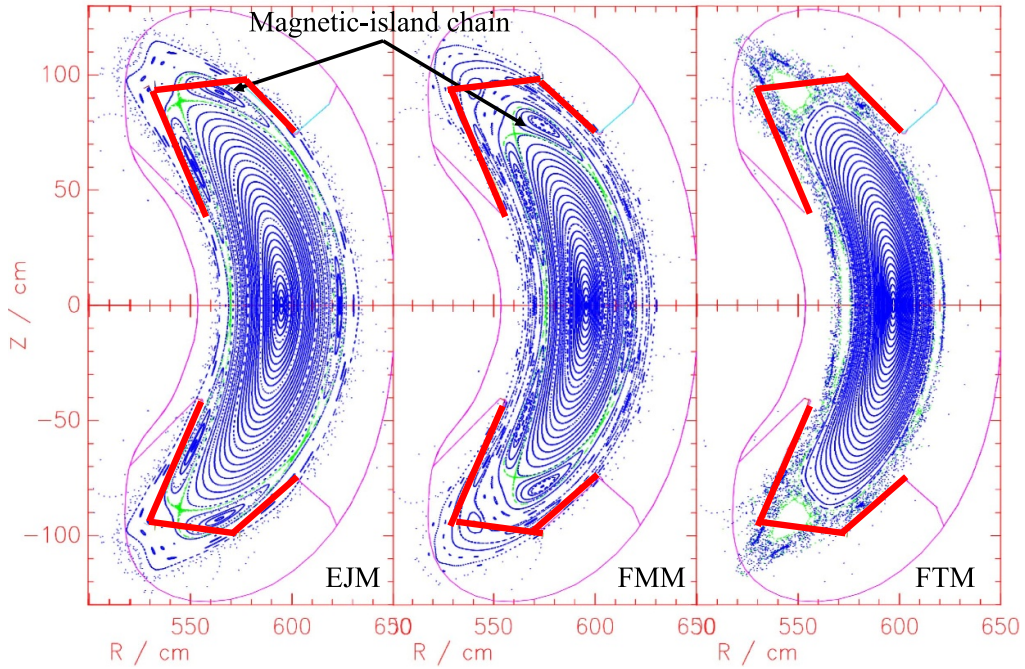

Figure 1. Poincaré plots showing vacuum calculations of the magnetic flux surfaces, including the internal magnetic island chain for the bean-shaped cross-section of W7-X for different values of iota, increasing from left to right. Corresponding details of these configurations are given in table 1. For the high-confinement configuration (in the middle), the island chain is already inside the confinement region as the last closed flux surface (LCFS) occurs outside.

Table 1. Magnetic configurations and experimental ID.

Exp. ID	Config. name	Config. label	ι_0	ι_e	Island-chain	Confinement region
#20 180 927.09	FTM001	high-iota	1.012 ± 0.005	1.194 ± 0.005	5/4	island-divertor
#20 180 927.15	FQM001		0.969 ± 0.005	1.171 ± 0.005	5/5	limiter
#20 180 927.16	FOM003		0.934 ± 0.005	1.099 ± 0.005	5/5	limiter
#20 180 927.17	FNM		0.926 ± 0.005	1.095 ± 0.005	5/5	limiter
#20 180 927.22	FMM002	high-confinement	0.911 ± 0.005	1.077 ± 0.005	5/5	limiter
#20 180 927.33	EJM004	standard	0.858 ± 0.005	0.972 ± 0.005	5/5	island-divertor

respect to the spatial resolution of the $T_e$profile being measured by the ECE diagnostic with a radial resolution of 1 cm–2 cm. The detailed observations from the iota scan experiments are discussed in the following sections.

3. Transport barrier

The experimental observation showed that during the iota scan, as the 5/5 internal island-chain was moved closer to LCFS (approximately at 0.522 m) from inside the plasma, such that the distance between LCFS and the island-chain is reduced, a strong T_e gradient starts to develop at the plasma edge region [18]. Figure 2(*a*) shows that for the high-confinement configuration, a transport barrier builds up (marked by black dashed line) in T_e at the plasma edge around the plasma minor radius of 0.369 m for an ECRH plasma as the edge pressure increases. The edge barrier is broken by subsequent crashes reminiscent of the edge localized modes (ELMs) in tokamaks and stellarators [19–22]. Further on, the effect of the transport barrier can be observed via the enhanced rate of increase of both the line integrated plasma density, n_e, measured with interferometer diagnostics, and the stored diamagnetic energy W_{dia}. We note that edge density profiles that provide sufficient spatial resolution to address a possible n_e pedestal are not yet available in this campaign. The H_{alpha} radiation levels measured with filterscopes decrease as the T_e transport barrier becomes stronger, followed by ELM-reminiscent crashes, also observed in H_{alpha} radiation.

The presence of transport barriers and ELM-reminiscent crash is independent of the heating and plasma parameters of the evolving small plasma current (approximately 100 A) and hence indicating that the magnetic configuration itself is the decisive quantity. The edge pedestal occurs independent of details of the heating power (on/off-axis ECRH, NBI) and the ELM-reminiscent behavior persists during pellet injection where each pellet triggers a crash. The subsequent improved core confinement, that is presumably related to peaked density profiles, therefore reduced ITG turbulence [23, 24]. Both

observations indicate that the island-related pedestal can be considered independent of the details of the core.

Three different configurations are chosen from the standard-to-high-iota scan in figure 2(*b*) to show the T_e profiles (only from the high field side ECE as the low field side is polluted by downshifted core emission), for the same heating power of 2 MW, and n_e of $\approx 3.5 \times 10^{19}\,\mathrm{m}^{-3}$, mapped to the plasma radius with the HINT code [25, 26] which includes the internal island-chain while estimating the equilibrium. The configurations shown in the figure are of limiter-type; FQM001 ($\iota_0 = 0.969$), FOM003 ($\iota_0 = 0.934$), and FMM002 ($\iota_0 = 0.911$) with the 5/5 island chain present inside the LCFS, while the distance to LCFS decreases, respectively. The transport barrier is present in these configurations with a gradual increase in pedestal height, with decreasing iota as the island chain moves closer to LCFS. Simultaneously, the core T_e increases as the transport barrier strengthens. For the high-confinement configuration, where the highest pedestal height is observed, the strongest gradients in the T_e profile appear around the plasma minor radius of 0.369 m (LCFS is located at approximately 0.522 m).

Localizing the pedestal with respect to the internal island chain is essential to understanding how the islands affect the transport in that layer. It is found that for the high-confinement configuration, the transport barrier forms not inside the island but rather in front of its inner boundary (location of the island shaded in red in figure 2(*b*)) toward the plasma core.

Table 2 provides the pedestal height for different sample limiter configurations from the scan for the same heating power of 2 MW, and n_e of $\approx 3.5 \times 10^{19}\,\mathrm{m}^{-3}$. The transport barrier is only present for the limiter configurations with an island chain inside the confinement region. No transport barrier related crashes near the plasma edge were observed for configurations with island chains outside the LCFS. The pedestal height increases as the island chain inside the plasma confinement region is moved toward the flux surface connected to the divertor. The barrier is linked to the island's location as it is in front of it rather than inside the island. The subsequent crashes breaking the transport barrier are discussed in the following section.

4. Crashes reminiscent to edge localized modes

For configurations with transport barriers, crashes were observed in multiple plasma diagnostic measurements as shown in figure 3, for example, in T_e, n_e, W_{dia}, toroidal current, I_{tor}, and H_{alpha} radiation. Figure 4 shows the cross-correlation of different ECE channels and W_{dia} to find the precise location of the crash as the pivot point of the T_e profile. The figures show that the crash occurs at a plasma minor radius of 0.369 m (marked in red in figure 2(*b*)), which is also the location of the transport barrier as shown in the previous section, and, hence, the crashes are a direct consequence of the excessive pressure buildup at the pedestal location. The heat wave propagation in the plasma caused by these crashes can be observed with an inverted phase of the crash in the neighboring T_e measurements (see figure 3, top plot) and additionally with a lag in the T_e crash at different locations in the plasma (see figure 4) as the heat wave propagates outwards from the location of the crash with decaying amplitude. The fast W_{dia} measurements show that a typical crash results in an energy loss of up to 5% [18]. Since these crashes occur because of the broken transport barrier and result in loss of stored energy, they are reminiscent of a tokamak ELMy crash. However, the transport barrier, unlike in a tokamak, is not present at the plasma edge but instead is linked to the location of the internal island chain, and, hence, the crashes have been referred to as island localized modes (ILMs) [27, 28]. The characteristics of these crashes, such as frequency and amplitude, were observed to change with magnetic island size and location, plasma density, plasma heating type, and power. This can be explained by the fact that the crash amplitude changes as soon as the pedestal pressure changes by external factors. As the crash is a consequence of the broken transport barrier, the amplitude of the crash depends on how strong the barrier is. Hence, the strongest crashes are observed in the high-confinement configuration with the highest T_e pedestal height.

5. Backward transition to a degraded confinement state

The T_e pedestal develops within a few tens of ms already during the startup phase of the plasma when the density is increased. A sudden forward transition to a high confinement state as observed in many devices has not been observed so far, however, this may be masked by the developing plasma conditions. This motivated us to look for a backward transition or how the transport barrier evolves during the plasma decay, which is not corrupted by some conditions which hinder the observation of the forward transition during plasma startup. Also, at W7-AS there was a clear backward transition observed in comparison to a forward transition [19].

As the plasma heating was stopped, during the plasma decay phase, a backward transition [6, 29] to a degraded confinement state for the configuration with transport barrier could be observed with multiple plasma diagnostics, for example, changed T_e edge gradients at the point of transition, increased H_{alpha} radiation levels (shown in figure 5) and faster decaying rate of stored energy as well as plasma density [18]. The typical fingerprints of a backward transition to a degraded confinement state observed in other helical devices are increased H_{alpha} radiation levels and changed W_{dia} rate [30, 31]. Pedestal density measurements are not available in sufficient quality to calculate the pedestal pressure at the transition and to compare the backwardtransition parameters for different configurations.

6. Impact on plasma confinement

The impact of the transport barrier on plasma confinement can be seen through the increased core T_e profile (figure 2(*b*)). Moreover, figure 6 shows a comparison of pedestal T_e, core

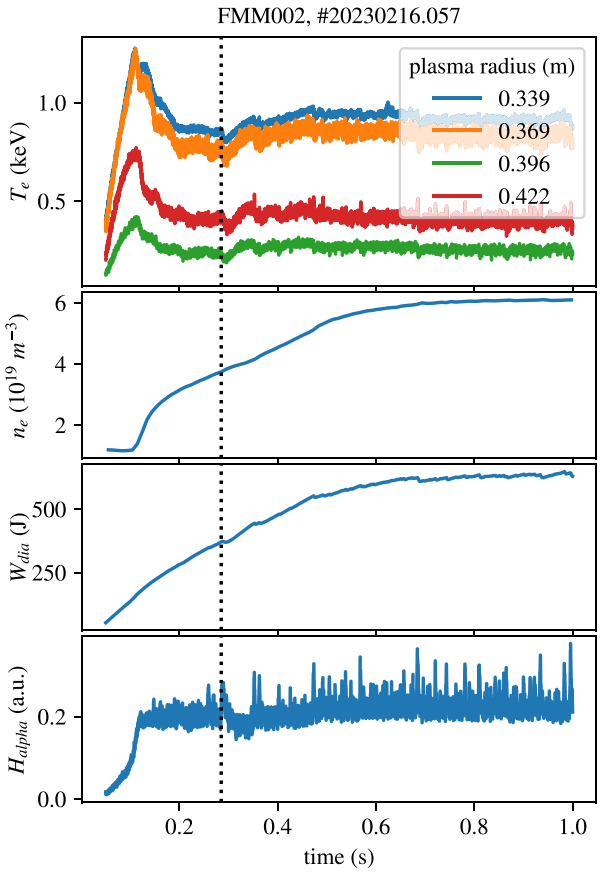

(a)

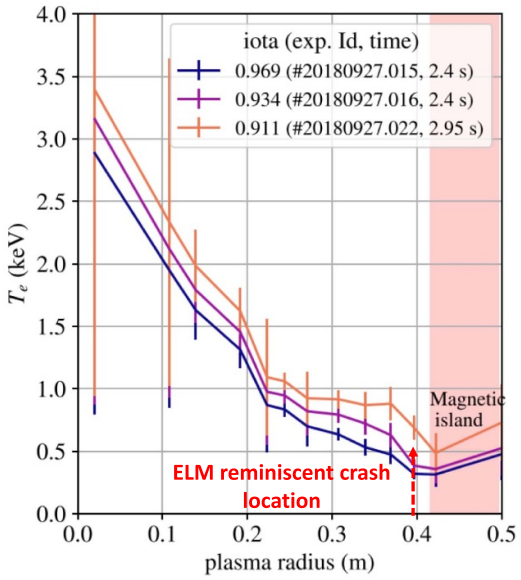

(b)

Figure 2. (*a*) Buildup of a transport barrier (marked with black dashed line) is shown in high confinement configuration, where the internal 5/5 island-chain is inside the LCFS, with the T_e (important to note that the radiation temperature of ECE is taken as T_e for these figures, and hence, the radial location and relative trends are of more importance than absolute values) at different plasma radius, the line integrated plasma density n_e, the stored diamagnetic energy W_{dia} and the H_{alpha} radiation levels. (*b*) The high field side T_e profiles from ECE for the high iota configuration scan at the heating power of 2 MW and a plasma density of $\approx 3.5 \times 10^{19}$ m^{-3}. The profile mapping is done with HINT equilibrium, including the island in the calculation. The magnetic island is ≈8 cm wide for high confinement configuration ($\iota_0 = 0.911$, FMM002, shaded in red) and is located around 0.416–0.496 m.

Table 2. T_e pedestal height.

Config. name	ι_0	T_e pedestal height $\approx$ (eV)
FQM001	0.969	158.50
FOM003	0.934	271.03
FNM	0.926	337.95
FMM002	0.911	394.91

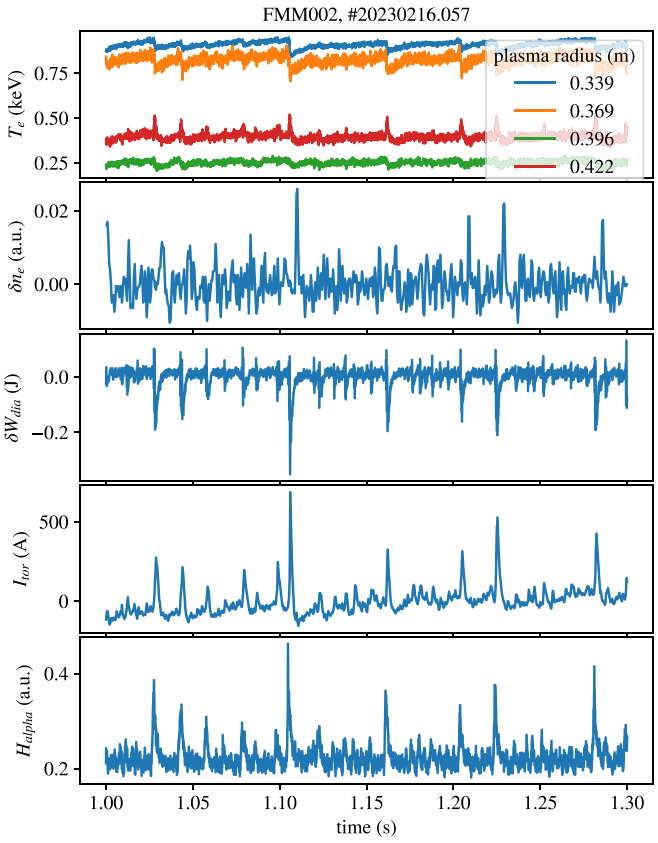

Figure 3. ELM-reminiscent crashes observed with multiple plasma diagnostics at W7-X for the high-confinement configuration. The spatially resolved local T_e measurement from the ECE diagnostic is used to localize the crashes with an inversion radius around 0.369 m (top plot). The crashes are also observed in line integrated density, n_e, measurement, W_{dia}, toroidal current, I_{tor}, and H_{alpha} radiation levels.

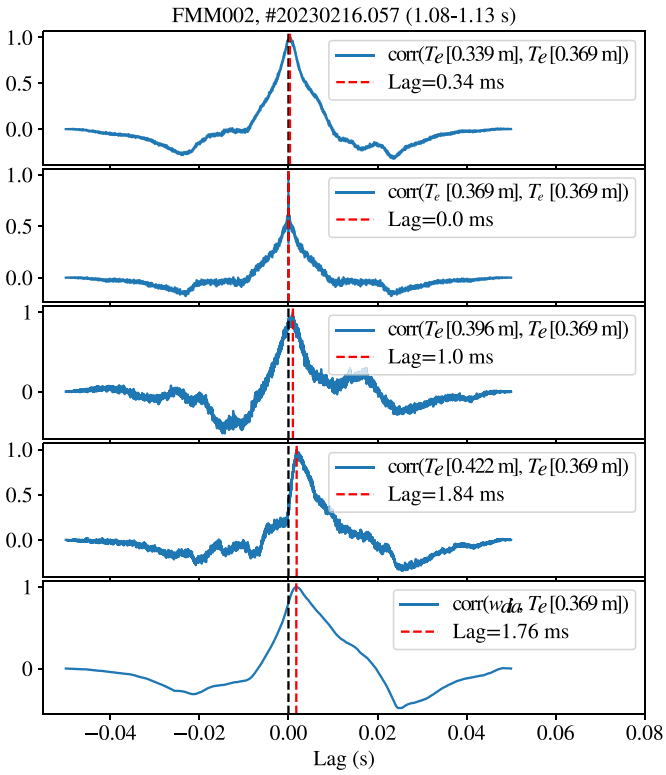

Figure 4. Cross-correlation of T_e at the inversion radius of crash, 0.369 m (second row of plot), with T_e at neighboring layers shown (top four plots) for the high-confinement configuration. The cross-correlation shows the outward propagating heat wave from the crash as there is a temporal lag (marked with the red dashed line) between different locations. The lowest plot shows the cross-correlation of W_{dia} with T_e at the inversion radius of the crash, and the effect of the crash is observed in W_{dia} after 1.76 ms.

7. Conclusion and discussion

T_e and W_{dia} for different configurations. The overall increase in W_{dia} for these configurations, which is also reported in [11], can be explained by the presence of a transport barrier resulting in increased core T_e profiles. The improvement in confinement is maximum as the island chain is closest to LCFS but not intersecting with divertor targets as shown in the figure with the highest W_{dia} for the lowest iota limiter configuration. Additionally, as a preliminary explanation behind the role of islands in the pedestal creation, the Doppler reflectometry diagnostic measured a strong W-shaped $E \times B$ shear [32] at the location of the island, indicating the presence of an $E \times B$ shear related transport barrier [5, 33–38]. A more detailed experimental investigation is planned for the next W7-X campaign with improved plasma edge diagnostics.

A magnetic configuration scan was performed at W7-X by varying the rotational transform between iota = 5/4 and iota = 5/6 at the plasma boundary to analyze the plasma confinement for magnetic configurations with different internal magnetic island sizes and locations. For the magnetic configurations, where the 5/5 island chain was moved inside LCFS, the spatially localized and highly temporally resolved ECE measurements showed that a T_e transport barrier develops during the plasma buildup phase and the barrier is broken by subsequent fast crashes which have characteristics like the tokamak ELMs. Heat wave propagation through ECE channels caused by ELM-reminiscent crashes can be observed with an inverted phase of signals in neighboring channels to the location of the crash. The magnetic island locations for these

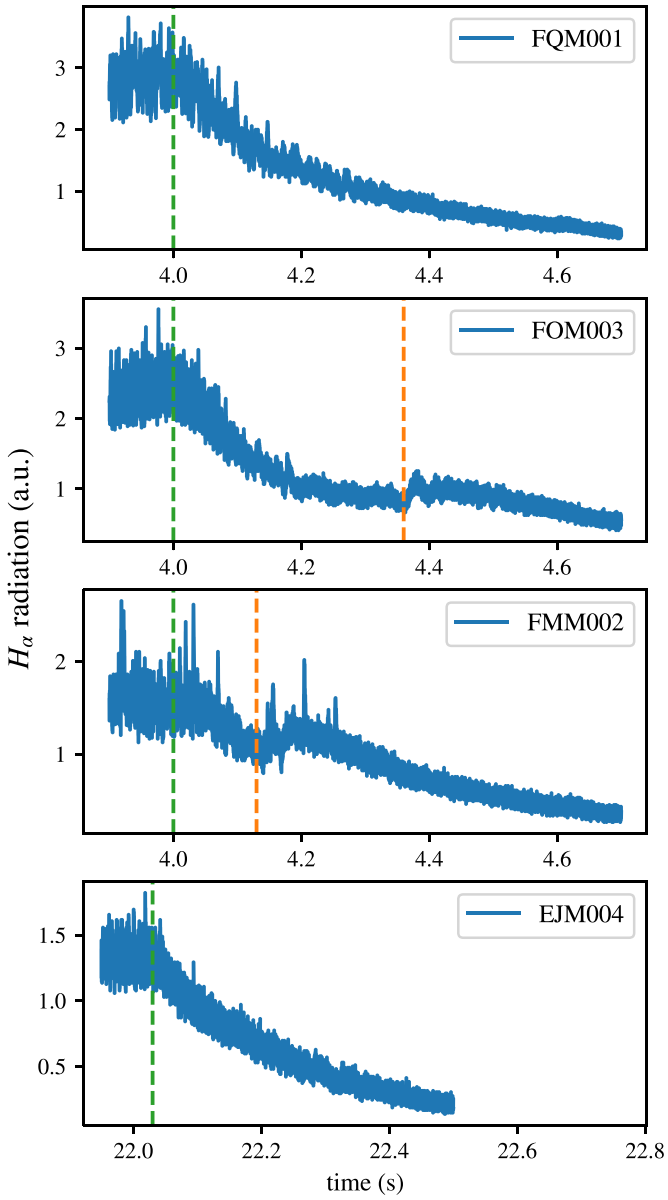

Figure 5. Backward transition (marked in orange dashed line) to a degraded confinement state is shown for the high-confinement and FOM003 (also a limiter configuration) configurations during the plasma decay phase after the heating was switched off (marked in green dashed line). The increased H_{alpha} radiation levels are used as a fingerprint of a backward transition to a degraded confinement state. The backward transition is also seen in the T_e gradients and W_{dia} decay rate [18].

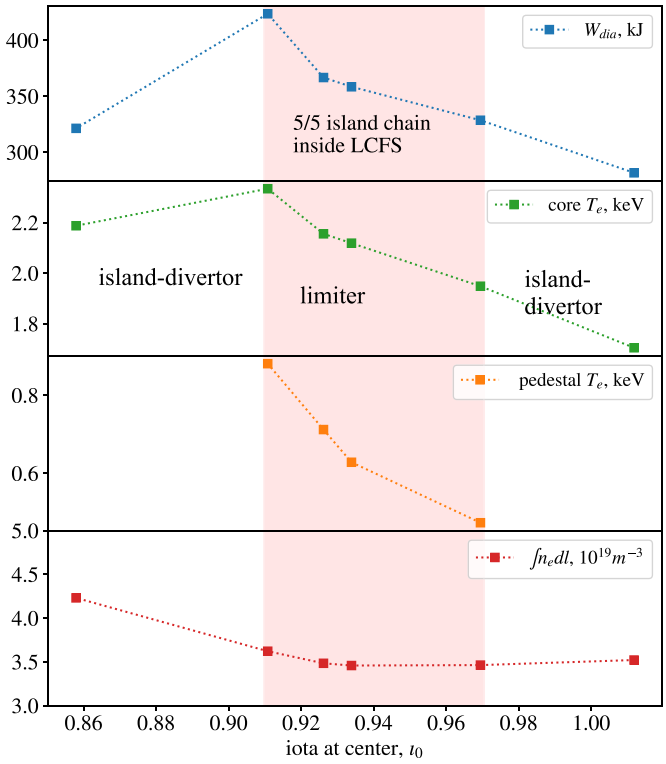

Figure 6. W_{dia}, core T_e, pedestal T_e and line integrated n_e are shown for high iota configuration scan from 5/5 island-divertor EJM004 ($\iota_0 \approx 0.858$) to 5/4 island-divertor FTM001 ($\iota_0 \approx 1.012$) at the same ECRH of 2 MW. The pedestal is only present for limiter configurations (shaded in red in the figure). The strongest transport barrier configuration FMM002 ($\iota_0 \approx 0.911$) with highest pedestal temperature also results in the highest W_{dia}.

configurations are derived from equilibrium calculations done with the HINT code. The mapping of the magnetic island and the T_e pedestal to the plasma minor radius showed that the transport barrier develops right before and not inside the inner boundary of the rational island toward the plasma core which suggests that islands affect the transport in that regime, and the location of the transport barrier is correlated with the iota profile and, hence, to the island's location. The magnetic island chain can be placed near the magnetic axis, but observations show that as the island chain is moved closer to the magnetic axis, the pedestal height starts to diminish, and consequentially, the confinement. ELM-reminiscent crashes were observed in multiple plasma diagnostic measurements, such as W_{dia}, toroidal current, magnetic fluctuations, and H_{alpha} radiation. The W_{dia} measurements show that a typical ELM-reminiscent crash can be accompanied by an energy loss of up to 5%. The characteristics of the crash, such as frequency and amplitude, were observed to change with magnetic island size and location, plasma heating method, and power and plasma density. In tokamaks, the magnetic resonant perturbations are used for ELM mitigation [39]. The observations in W7-X support the observation that islands influence the transport in neighboring layers in a magnetic confinement device and can be exploited as a tool to optimize shear for improved confinement.

The impact of the transport barrier on plasma confinement can be seen through the increased core T_e profile, which could explain the overall increase in W_{dia} for these configurations. Additionally, as a possible preliminary explanation behind the role of islands in the pedestal creation, a strong W-shaped $E \times B$ shear inside the island was observed that supports the presence of a shear-related transport barrier [32]. The presence of the localized radial E well in an island have been linked to the formation of internal transport barriers, for example, in [38], the island-induced $E \times B$ shear layer alongside sheared vortex flows results in internal transport barrier formation through local turbulence suppression in the inner core region next to the island and simultaneously preventing

the turbulence to spread from the outside to the inside of shear layer. The pedestal builds up already during the plasma start-up phase in the W7-X stellarator, and, hence, no clear forward transition is observed for the available configurations with different iota profiles; however, a backward transition to a degraded confinement state is observed during the plasma decay phase. In W7-X, details of the heat load to the divertors in these high-confinement configurations are still under investigation. Also, the maximum plasma discharge length in these essentially limiter configurations is 10 s such that the detachment is not yet a necessary precondition to obtain a stationary plasma discharge. We note that the theoretical understanding of a transport barrier linked to an internal island still needs further clarification. This is of particular relevance for low-shear stellarator devices and their well known iota dependence on transport, as in these devices lower-order rationals are radially better separated and external magnetic perturbations or higher-order components of the magnetic spectrum at the location of these rationals may initiate or blow up islands with a finite width. However, a more detailed understanding still needs further clarification: while in W7-AS low order rationals passed with low magnetic shear, constituting a kind of transport, shortcuts were considered to be responsible for a degradation of confinement at certain iota values [4]. Other experiments like TJ-II found rationals to be related to mini transport barriers speculating that they constitute local flow shear regions [40]. In this discussion, this paper provides indications that a macroscopic $E \times B$ shear-flow related transport reduction may be related or initialized by an island chain.

Internal magnetic islands, as they may be initiated in low shear stellarators, have often been considered as transport shortcuts that have to be avoided. However, rational surfaces are linked to triggering of internal transport barriers via generation of the $E \times B$ flow shear in both tokamaks and stellarators [33, 41–43] and the corresponding investigation of the role of the $E \times B$ flow shear structure in creation of transport barriers is reported in [44, 45]. In stellarators, for example: in a large helical device, the low order rational surfaces are linked to transport barrier formation, L-H transition and consequentially improved confinement [46, 47]; in Heliotron-J, the presence of a low order rational at the location of an electron transport barrier was found to expand the improved confinement region [48] and in TJ-II, $E \times B$ flow shear was reported to be correlated to the rational surfaces [43, 49] and a transition to improved core heat confinement triggered by the low order rational surfaces was also reported [50]. The experimental observations in W7-X limiter configurations also show a similar effect of edge magnetic islands on transport with generation of $E \times B$ flow shear [32] which results in strong profile gradients and edge electron transport barriers with reduced transport and improved confinement. Additionally, W7-X observations also show relaxation of transport barriers via fast ELM-reminiscent crashes correlated to the magnetic island location. Similar observations of ELM-reminiscent edge bursts at low order rational locations are reported at the TJ-II stellarator [51] and ELM-reminiscent crashes have also been reported from other stellarators [19, 52]. In a stellarator, island size and location can be controlled, and, hence, islands or rational surfaces provide a configuration tool to tailor such high confinement states; however, with side effects such as wall loads from ELM-reminiscent crashes, which need to be taken into account.

Acknowledgments

This work has been carried out within the framework of the EUROfusion Consortium, funded by the European Union via the Euratom Research and Training Programme (Grant Agreement No. 101052200 - EUROfusion). Views and opinions expressed are however those of the author(s) only and do not necessarily reflect those of the European Union or the European Commission. Neither the European Union nor the European Commission can be held responsible for them.

ORCID iDs

N. Chaudhary https://orcid.org/0000-0001-5075-2487
M. Hirsch https://orcid.org/0000-0002-7120-6087
T. Andreeva https://orcid.org/0000-0003-2390-4240
J. Geiger https://orcid.org/0000-0003-4268-7480
R.C. Wolf https://orcid.org/0000-0002-2606-5289
G.A. Wurden https://orcid.org/0000-0003-2991-1484

References

[1] Wagner F. *et al* 1994 H-mode of W7-AS stellarator *Plasma Phys. Control. Fusion* **36** A61
[2] Erckmann V. *et al* 1993 H mode of the W7-AS stellarator *Phys. Rev. Lett.* **70** 2086
[3] Hirsch M. *et al* 2008 Major results from the stellarator Wendelstein 7-AS *Plasma Phys. Control. Fusion* **50** 053001
[4] Brakel R. (W7-AS Team) 2002 Electron energy transport in the presence of rational surfaces in the Wendelstein 7-AS stellarator *Nucl. Fusion* **42** 903
[5] Sano F. *et al* 2005 H-mode confinement of Heliotron J *Nucl. Fusion* **45** 1557
[6] Estrada T. and Hidalgo C. 2023 H-mode transition in the TJ-II stellarator plasmas *Phil. Trans. R. Soc.* A **381** 20210229
[7] Klinger T. *et al* 2019 Overview of first Wendelstein 7-X high-performance operation *Nucl. Fusion* **59** 112004
[8] Beidler C. *et al* 2021 Demonstration of reduced neoclassical energy transport in Wendelstein 7-X *Nature* **596** 221–6
[9] Wolf R. *et al* 2018 Electron-cyclotron-resonance heating in Wendelstein 7-X: a versatile heating and current-drive method and a tool for in-depth physics studies *Plasma Phys. Control. Fusion* **61** 014037
[10] Otte M. *et al* 2016 Setup and initial results from the magnetic flux surface diagnostics at Wendelstein 7-X *Plasma Phys. Control. Fusion* **58** 064003
[11] Andreeva T. *et al* 2022 Magnetic configuration scans during divertor operation of Wendelstein 7-X *Nucl. Fusion* **62** 026032
[12] Feng Y., Sardei F., Kisslinger J., Grigull P., McCormick K. and Reiter D. 2004 3D Edge Modeling and Island Divertor Physics *Contrib. Plasma Phys.* **44** 57–69
[13] Feng Y. *et al* 2021 Understanding detachment of the W7-X island divertor *Nucl. Fusion* **61** 086012
[14] Pedersen T.S. *et al* 2018 First results from divertor operation in Wendelstein 7-X *Plasma Phys. Control. Fusion* **61** 014035
[15] Geiger J. *et al* 2021 Confinement and equilibrium with internal islands in a configuration scan with respect to iota in W7-X

Preprint: 28th IAEA Fusion Energy Conf.(FEC-2020, Virtual Event) (Nice, France, 10–15 May 2021) (available at: https://nucleus.iaea.org/sites/fusionportal/Shared%20Documents/FEC%202020/fec2020-preprints/preprint0803.pdf)
[16] Andreeva T. *et al* 2019 Equilibrium evaluation for Wendelstein 7-X experiment programs in the first divertor phase *Fusion Eng. Des.* **146** 299–302
[17] Hirsch M. *et al* 2019 ECE diagnostic for the initial operation of Wendelstein 7-X *EPJ Web Conf.* **203** 03007
[18] Chaudhary N. *et al* 2023 Radial localization of electron temperature edge pedestal and ELM-like events using ECE measurements at Wendelstein 7-X *EPJ Web Conf.* **277** 03004
[19] Hirsch M. *et al* 2000 Operational conditions and characteristics of ELM-events during H-mode plasmas in the stellarator W7-AS *Plasma Phys. Control. Fusion* **42** A231
[20] García-Cortés I. *et al* 2000 Edge-localized-mode-like events in the TJ-II stellarator *Nucl. Fusion* **40** 1867
[21] Grigull P. *et al* 2001 Edge transport barrier formation and ELM phenomenology in the W7-AS stellarator *J. Nucl. Mater.* **290** 1009–12
[22] Zohm H. 1996 Edge localized modes (ELMs) *Plasma Phys. Control. Fusion* **38** 105
[23] Maassberg H. *et al* 2000 The neoclassical 'electron root' feature in the Wendelstein-7-AS stellarator *Phys. Plasmas* **7** 295–311
[24] Zoletnik S., Basse N., Saffman M., Svendsen W., Endler M., Hirsch M., Werner A. and Fuchs C. (the W7-AS Team) 2002 Changes in density fluctuations associated with confinement transitions close to a rational edge rotational transform in the W7-AS stellarator *Plasma Phys. Control. Fusion* **44** 1581
[25] Harafuji K., Hayashi T. and Sato T. 1989 Computational study of three-dimensional magnetohydrodynamic equilibria in toroidal helical systems *J. Comput. Phys.* **81** 169–92
[26] Suzuki Y., Nakajima N., Watanabe K., Nakamura Y. and Hayashi T. 2006 Development and application of HINT2 to helical system plasmas *Nucl. Fusion* **46** L19
[27] Wurden G. *et al* 2019 Structure of island localized modes in Wendelstein 7-X *46th EPS Conf. on Plasma Physics (EPS-2019)* (*Milan, Italy, 8–12 July 2019*) P2.1068 (available at: http://ocs.ciemat.es/EPS2019PAP/pdf/P2.1068.pdf)
[28] Wurden G.A. *et al* 2022 A special case of long-pulse high performance operation in W7-X *48th EPS Conf. on Plasma Physics (EPS-2022)* (*Online, 27 June–01 July 2022*) P1b.118 (available at: https://info.fusion.ciemat.es/OCS/eps2022pap/pdf/P1b.118.pdf)
[29] Wagner F. *et al* 2003 Major results from Wendelstein 7-AS stellarator *19th IAEA Fusion Energy Conf.* (*Lyon, France, 14–19 October 2002*) IAEA-CN-94/OV/2-4 (available at: https://www-pub.iaea.org/MTCD/publications/PDF/csp_019c/pdf/ov2_4.pdf)
[30] Hirsch M., Akiyama T., Toi K., Estrada T., Hidalgo C., and Mizuuchi T. 2010 H-mode in helical devices *IAEA-CN–180* (International Atomic Energy Agency (IAEA))
[31] Wagner F., Hirsch M., Hartfuss H., Laqua H. and Maassberg H. 2006 H-mode and transport barriers in helical systems *Plasma Phys. Control. Fusion* **48** A217
[32] Estrada T. *et al* 2021 Impact of magnetic islands on plasma flow and turbulence in W7-X *Nucl. Fusion* **61** 096011
[33] Ida K. *et al* 2004 Radial electric field and transport near the rational surface and the magnetic island in LHD *Nucl. Fusion* **44** 290
[34] Kitajima S. *et al* 2006 Effects of rational surfaces and magnetic islands on radial electric fields and ion viscosity in tohoku university heliac *Fusion Sci. Technol.* **50** 201–6
[35] Chechkin V. *et al* 2006 Processes arising in the edge and diverted plasmas during ITB formation in the U-3M torsatron *Plasma Phys. Control. Fusion* **48** A241
[36] López-Bruna D. *et al* 2011 Magnetic resonances and electric fields in the TJ-II heliac *Plasma Phys. Control. Fusion* **53** 124022
[37] Kenmochi N. *et al* 2020 Reformation of the electron internal transport barrier with the appearance of a magnetic island *Sci. Rep.* **10** 5
[38] Wang W., Yoo M., Startsev E., Ethier S. and Chen J. 2021 Effects of magnetic islands on plasma confinement and self-driven current generation *Preprint: 28th IAEA Fusion Energy Conf.(FEC-2020, Virtual Event)* (*Nice, France, 10–15 May 2021*) (available at: https://nucleus.iaea.org/sites/fusionportal/Shared%20Documents/FEC%202020/fec2020-preprints/preprint1325.pdf)
[39] Suttrop W. *et al* 2018 Experimental conditions to suppress edge localised modes by magnetic perturbations in the ASDEX upgrade tokamak *Nucl. Fusion* **58** 096031
[40] Van Milligen B.P. *et al* 2018 Study of radial heat transport in W7-X using the transfer entropy *Nucl. Fusion* **58** 076002
[41] Joffrin E. *et al* 2003 Internal transport barrier triggering by rational magnetic flux surfaces in tokamaks *Nucl. Fusion* **43** 1167
[42] Ida K. *et al* 2001 Observation of plasma flow at the magnetic island in the Large Helical Device *Phys. Rev. Lett.* **88** 015002
[43] Pedrosa M. *et al* 2000 Role of rational surfaces on fluctuations and transport in the plasma edge of the TJ-II stellarator *Czech. J. Phys.* **50** 1463–70
[44] Fujisawa A. 2004 Internal transport barrier and bifurcation phenomena in stellarators *Fusion Sci. Technol.* **46** 91–100
[45] Burrell K., Austin M., Greenfield C., Lao L., Rice B., Staebler G. and Stallard B. 1998 Effects of velocity shear and magnetic shear in the formation of core transport barriers in the DIII-D tokamak *Plasma Phys. Control. Fusion* **40** 1585
[46] Toi K., Tanaka K., and Watanabe F. 2010 Role of low-order rational surfaces in transport barrier formation on the large helical device *Technical Report* (National Inst. for Fusion Science)
[47] Toi K. *et al* 2006 Formation of edge transport barriers by L-H transition and large reversed plasma current on LHD *Plasma Sci. Technol.* **8** 5
[48] Minami T. *et al* 2018 Effect of magnetic field structure on electron internal transport barrier and its role for the barrier formation in Heliotron J *27th IAEA Fusion Energy Conf. (FEC 2018)* (*Gandhinagar, India, 22–27 October 2018*) (available at: https://nucleus.iaea.org/sites/fusionportal/Shared%20Documents/FEC%202018/fec2018-preprints/preprint0063.pdf)
[49] Estrada T., Ascasíbar E., Blanco E., Cappa A., Hidalgo C., Ida K., López-Fraguas A. and van Milligen B.P. 2016 Plasma flow, turbulence and magnetic islands in TJ-II *Nucl. Fusion* **56** 026011
[50] Estrada T. *et al* 2007 Transitions to improved core electron heat confinement triggered by low order rational magnetic surfaces in the stellarator TJ-II *Nucl. Fusion* **47** 305
[51] de la Cal E. *et al* 2015 Edge localised mode-like instability driven plasma edge burst study in the TJ-II stellarator *Plasma Phys. Control. Fusion* **57** 075001
[52] Toi K., Ohdachi S., Ogawa K. and Suzuki Y. (LHD Experiment Group) 2018 Precursors and control of ELMs in stellarator/helical plasmas *A3 foresight program seminar on critical physics issues specific to steady state sustainment of high-performance plasmas 2017* (*Sapporo, Hokkaido (Japan), 11–14 July 2017*) p. 34-40 (available at: https://inis.iaea.org/collection/NCLCollectionStore/_Public/50/040/50040077.pdf)